HHS Public Access

Author manuscript

Int J Obes (Lond). Author manuscript; available in PMC 2016 October 22.

Published in final edited form as:

Int J Obes (Lond). 2016 August ; 40(8): 1292–1300. doi:10.1038/ijo.2016.43.

Diffuse optical spectroscopic imaging of subcutaneous adipose tissue metabolic changes during weight loss

Goutham Ganesan[a,b], **Robert V. Warren**[a], **Anaïs Leproux**[a], **Montana Compton**[a], **Kyle Cutler**[a], **Sharine Wittkopp**[d], **Gerard Tran**[a], **Thomas O'Sullivan**[a], **Shaista Malik**[c], **Pietro R. Galassetti**[b], and **Bruce J. Tromberg**[a,b]

[a]UC Irvine Beckman Laser Institute and Medical Clinic, 1002 Health Sciences Rd, Irvine, CA 92617

[b]UC Irvine Institute for Clinical and Translational Science, 843 Hewitt Hall, Irvine, CA 92617

[c]UC Irvine Department of Medicine, Division of Cardiology, 333 City Blvd. West, Suite 400, Orange, CA 92868

[d]UC Irvine School of Medicine, 25 Irvine Hall, Irvine, CA 92617

Abstract

Background—Changes in subcutaneous adipose tissue (AT) structure and metabolism have been shown to correlate with the development of obesity and related metabolic disorders. Measurements of AT physiology could provide new insight into metabolic disease progression and response to therapy. An emerging functional imaging technology, Diffuse Optical Spectroscopic Imaging (DOSI), was used to obtain quantitative measures of near infrared (NIR) AT optical and physiological properties.

Methods—10 overweight or obese adults were assessed during three-months on calorie-restricted diets. DOSI-derived tissue concentrations of hemoglobin, water, and lipid and the wavelength-dependent scattering amplitude (A) and slope (b) obtained from 30 abdominal locations and three time points (T0, T6, T12) were calculated and analyzed using linear mixed effects models, and were also used to form 3D surface images.

Results—Subjects lost a mean of 11.7 ± 3.4% of starting weight, while significant changes in A (+0.23 ± 0.04 mm^{-1}, adj. $p < 0.001$), b (−0.17 ± 0.04, adj. $p < 0.001$), tissue water fraction (+7.2 ± 1.1%, adj. $p < 0.001$) and deoxyhemoglobin [HbR] (1.1 ± 0.3 μM, adj. $p < 0.001$) were observed using mixed effect model analysis.

Discussion—Optical scattering signals reveal alterations in tissue structure which possibly correlate with reductions in adipose cell volume, while water and hemoglobin dynamics suggest

Corresponding author: Bruce J. Tromberg, 1002 Health Sciences Rd., Irvine, CA 92617. Phone: (949) 824-8705 bjtrombe@uci.edu.

Conflict of Interest declaration: BJT is a co-inventor of the DOSI technology described in this paper, the patents for which are owned by the regents of the University of California. Some of these patents have been licensed to private companies, and none of the authors have any financial interest with these entities. This research was conceived and performed with no contribution or assistance from these entities.

improved AT perfusion and oxygen extraction. These results suggest that DOSI measurements of NIR optical and physiological properties could be used to enhance understanding of the role of AT in metabolic disorders and provide new strategies for diagnostic monitoring of obesity and weight loss.

Introduction

Recent physiological studies have revealed the potentially critical role of adipose tissue (AT) in the development of metabolic disorders (1, 2). Both visceral and subcutaneous AT are subject to various pathophysiological processes, such as inflammation (3, 4), dysregulated oxygenation (5–8), and disrupted endocrine signaling (9, 10). Despite the importance of AT in disease, there are no widely-used methods for assessing AT physiology in humans. This work examines whether diffuse optical spectroscopic imaging (DOSI) could address this need. To that end, we have performed measurements on 10 overweight volunteers undergoing calorie restriction (CR) for weight reduction over a 12-week period.

CR has been shown to extend life span and reduce incidence of obesity-related complications in mammals, and these effects are mediated in part by changes in AT (11). In mice, three months of CR can lead to nitric oxide (NO) mediated increases in white AT mitochondrial DNA, peroxisome proliferator-activated receptor–γ coactivator 1α (PGC-1α), and markers of mitochondrial biogenesis (12). The authors of this study suggest that enhanced white AT SIRT0 expression contributes to the pro-longevity effects of CR in mammals (12).

Studies of CR in humans have reported morphological changes in AT, such as adipocyte size changes and altered profile of inflammatory cells (13). Specifically, weight reduction by CR causes adipocyte shrinkage; in a recent study, a 10% weight loss was shown to result in a 16% decrease in adipocyte volume (14), whereas another study showed high-fat diet increasing adipocyte volume in a matter of weeks (15). In humans, one recent study found a strong positive correlation between adipocyte size and the presence of Diabetes risk factors in bariatric surgery candidates (16). Another recent study revealed a correlation between adipocyte hypertrophy and both insulin resistance and AT inflammation (17).

It is also possible that adipocyte size changes influence cellular metabolism. For example, some data suggest a relationship between adipocyte size and AT angiogenesis (18). More important is the hypothesized relationship between adipocyte size and O_2 delivery (19). The diameters of hypertrophic adipocytes are thought to exceed the diffusion distance of O_2, causing lower cellular P_{O2} (19). Low PO_2 has been observed as a feature of obese AT in most studies (19), but there are conflicting reports. Importantly, there are data to suggest that it is in fact increased AT P_{O2} that is associated with inflammation and insulin resistance in obesity (5). A recent investigation in mice found that expression of hypoxia-inducible factor (HIF)-1 alpha increased in animals fed a high-fat diet, in response to *increased* AT O_2 consumption (6). Other investigations have focused on characterization of “beige” adipocytes, which consume more O_2 and are thought to correlate with enhanced metabolic health (20, 21).

Given the potential importance of the AT in metabolic disease, there is increased need for tools to characterize and image it. DOSI may be uniquely suited to this purpose. DOSI quantitatively measures interactions of near-infrared light with tissues at depth (22). It measures tissue reduced scattering (μ_s') and absorption (μ_a) coefficients, which are used to calculate tissue concentrations of oxyhemoglobin [HbO_2], deoxyhemoglobin [HbR], water, and bulk lipid fractions (23, 24). Together, these quantities reflect aspects of tissue perfusion, metabolism, hydration and total blood volume (25). Similar techniques are increasingly used in the study of cerebral (26) and muscular (27) hemodynamics and metabolism, as well as in cancer biology (28), but to this date have not been applied to AT.

There were two specific hypotheses: 1. that CR would be associated with changes in tissue scattering parameters, consistent with a reduction in adipocyte size, as well as a potential increase in density of subcellular components; and 2. that CR would be associated with a change in metabolic profile in subcutaneous AT, defined primarily by changes in [HbR], [HbO_2] and water content, DOSI-derived parameters that correlate with changes in tissue blood flow and metabolic rate of oxygen consumption (22, 28).

Subjects and Methods

Subjects and experimental design

Participants were recruited from a medically-supervised weight management program. Measurements occurred at the Beckman Laser Institute (BLI) and Medical Clinic at UC-Irvine (Irvine, CA). Males and females 18–75 years old were included. Measurement sessions occurred thrice: T0 (before or within two weeks of starting weight loss), T6 (6–8 weeks after T0), and T12 (6 weeks after T6). At each session, subjects were assessed for weight, blood pressure, abdominal circumference, diet and physical activity. Blood pressure was obtained while supine, after 10 minutes of rest. A total of 11 subjects participated in this study, of which 1 subsequently withdrew voluntarily, resulting in an n = 10 (5 M, 5 F). Subsequent measurement sessions occurred at the same time of day as the initial, and subjects were instructed to maintain the same daily schedule on all measurement days with regard to meal timing and physical exertion.

Calorie Restriction

Weight loss was achieved through medically supervised calorie restriction by meal replacement (HMR 70 program, MA, USA). Two levels of calorie restriction were administered in this group of subjects (Table 1), according to subject preference. The more restrictive plan (type 1) involved intake of between 500–800 kcal/day, while the more flexible plan (type 2) allowed for up to 1200 kcal/day. Exercise during the program was not controlled, but regular low to moderate exertion was encouraged. The rates of weight loss experienced therefore varied between subjects, as did the initial degree of overweight.

Ultrasound Measurements

Ultrasound images were performed at each of the 10 middle row grid points using an HDI-5000 imaging unit (Phillips Healthcare, MA, USA). Subsequently, subcutaneous tissue thickness was measured using the unit’s built-in software. Tissue thickness was defined as

the distance from the surface of the skin to the most superficial visible muscle layer. Thickness values were recorded and analyzed at all three measurement sessions.

DOSI Measurements

With each participant supine, a skin marker was used to draw a rectangular grid of 30 points centered about the umbilicus. The grid consisted of 3 horizontal rows separated by 4 cm, and 10 columns separated by 3 cm (Figure 1A). After at least 10 minutes of rest, 3 DOSI measurements were obtained at each grid point and averaged for analysis. Grid points were named by row (U for upper, M for middle, L for lower), and column (1–10).

The full technical details of DOSI are described elsewhere (23, 24, 29, 30). Briefly, DOSI consists of two parallel optical measurement modalities. One, frequency-domain photon migration (FDPM) uses modulated laser sources (50 – 500 MHz) of four wavelengths (660, 690, 780, and 830 nm), while the second broadband NIRS system makes use of white light source and spectrophotometer to provide 650–1000 nm broadband reflectance data. FDPM and NIRS signals are combined using a model-based approach to obtain quantitative tissue NIR absorption and scattering spectra.

Detector and source fibers encased in a plastic housing were placed on the surface of the skin at a source-detector separation of 22 mm. At each measurement point, reflected signals were collected, and analyzed using custom software (21) in MATLAB (Mathworks, MA, USA). The FDPM system detects phase and amplitude of reflected modulated light, and after calibration against a silicone phantom, fits this information to the diffusion equation (24) to obtain tissue absorption (μ_a) and reduced scattering (μ_s') coefficients. Then, the broadband diffuse reflectance signal was fit to the measured FDPM optical properties to obtain μ_a and μ_s' at all wavelengths (650–1000 nm). Finally, concentrations of oxyhemoglobin ([HbO_2]), deoxyhemoglobin ([HbR]), total hemoglobin ([THb]), and fractions of water and lipid were calculated using least-squares method and known molar extinction coefficients. Oxygen saturation (stO_2, [HbO_2]/[THb]) was also calculated. Both raw μ_a and μ_s' spectra were also obtained and used for analysis and visualization.

Image Generation

After initial processing, DOSI data from each session was plotted using grid coordinates and heat map functions in MATLAB. Linear interpolation was used to account for sparse spacing of grid points. The colored maps were overlayed on a 3D textured mesh of a one representative abdomen with grid points drawn on it. The initial 3D image was obtained by using Kinect for windows and accompanying software development kit (Microsoft, WA, USA). Colored heat maps obtained from MATLAB were warped and overlayed on the textured mesh using Photoshop CS6 Extended (Adobe, CA, USA) to create the final images.

Monte Carlo Simulations

Monte Carlo simulations were performed to assess optical penetration depth with an open-source Monte Carlo command line application (31) (version 2.0.1, URL: http://virtualphotonics.codeplex.com/releases/). A three-layered, semi-infinite geometry representing an upper skin layer (2 mm), a middle adipose layer (10 – 25 mm), and a bottom

semi-infinite layer of muscle was simulated to determine to what probability the detected photons interrogate each layer. One million photon trajectories were simulated from a source separated 22 mm from the detector, mimicking the DOSI instrument used in this study. The optical properties of each layer at 800nm were specified as reported from previous studies (32, 33). In particular, for skin, adipose, and muscle respectively: μ_a values were 0.025, 0.004, and 0.07 mm^{-1}; μ_s' values were 2.5, 1.9, and 0.7 mm^{-1}; g values were 0.8, 0.8, 0.95; and n was fixed at 1.4 for all three tissue types.

Statistics

Statistical analysis was performed using R (R Core Team (2014). R: A language and environment for statistical computing. R Foundation for Statistical Computing, Vienna, Austria. URL http://www.R-project.org/). Optical and ultrasound data were analyzed using the lme4 package (version 1.1–7, URL: http://CRAN.R-project.org/package=lme4) for computation of linear mixed-effects model (34). The basic model used was of the following form (35, 36):

$$Y_{ij}=\beta_0+\beta_1(X_i)+b_{0ij}+b_{1ij}(X_{ij})+b_{2ik}+b_{3ik}(X_{ik})+\varepsilon \quad \text{(M1)}$$

$$i=1,2,3 \quad j=1,2\ldots10 \quad \mathrm{k}=1,2\ldots30$$

where X_i is the effect of calorie restriction (CR), X_{ij} is the effect of CR (i = 1–3 levels) for individual subjects (j = 1–10), and X_{ik} is the effect of CR for individual positions (k = 1–30). Y_{ij} describes the value of an outcome variable for subject j at level of CR i. We modeled CR as a fixed effect and assigning it a categorical factor reflecting duration, with three levels *i* (T0 = 0 weeks of CR, T6 = 6–8 weeks of CR, T12 = 12–14 weeks of CR). The effect of CR is therefore described by β_1, with β_0 corresponding to fixed effect intercept. Model M1 also accounts for random effects of subject and position. Subject random effects are described by intercept b_{0ij} and slope b_{1ij}. Position random effects are modeled as intercept b_{2ik} and slope b_{3ik}. For each outcome, a value for β_1 for each level of CR and corresponding *p*-values are reported in supplementary table S1. If M1 revealed significant effects of CR on a given outcome variable, model output was used to perform Tukey's contrasts for multiple comparisons between mean values for all subjects at the three measurement sessions, as described in the results. Outcomes evaluated using this model included A, b, [HbO_2], [HbR], [THb], stO_2, water content, and lipid content. Model assumptions (linearity and normality) for each outcome was tested by visually inspecting plots of model residuals against fitted values, and by assessment of Q-Q plots respectively.

Prior to model analysis, DOSI measurements at two points were excluded from analysis due to unphysical optical properties, likely a result of improper probe contact. Additionally, 11 measurements from one session (T0) in subject 9 were missing due to instrument malfunction. Pearson Product-Moment Correlation analysis was used to test the mean change in each optical parameter from T0–T12 against the percentage of starting weight lost by each participant.

The effect of CR on weight, abdominal circumference, and blood pressure was tested by Friedman's test and post-hoc pairwise Wilcoxon rank-signed tests with Bonferroni correction.

Approval

This study was approved by the UC Irvine Institutional Review Board, and written informed consent was obtained from each participant before any study procedures were conducted.

Results

Subject characteristics

Participant data, means, and Wilcoxon p-values are shown in table 1. Mean weight loss was larger between T0 and T6 (−7.9 kg) than between T6 and T12 (−4.4 kg). From T0 to T12, the mean reduction in weight was 11.7 ± 1.1 % (SE) of starting weight. Systolic blood pressure declined by 8 mm Hg between T0 and T6 (adj. $p = 0.017$).

Adipose thickness and optical penetration depth

Tissue thicknesses obtained from ultrasound measurements at all points for all subjects are summarized in supplementary figure S1. Mean tissue thickness at T0 was 3.3 cm, and changed significantly at both T6 and T12 (T6 – T0 = 0.3 ± 0.1 cm, adj. $p < 0.001$, T12 – T0 = 0.5 ± 0.1 cm, adj. $p < 0.001$, T12 – T6 = 0.3 ± 0.1 cm, adj. $p < 0.001$). In terms of position, the subcutaneous fat layer was consistently thicker at positions closer to the midline. Simulation of photon penetration revealed a mean interrogation depth of 5–6 mm, with less than 4% signal contribution from tissue more than 1.0 cm deep (Supplementary figure 2).

DOSI measurements and images

A total of 30 sites on the abdomen were measured for each subject at each visit, centered about the umbilicus (figure 1A). Using all measurements, heat maps were generated overlying a 3D geometry representing the abdomen (figure 1B). For further analysis, at each measurement point, NIR spectra for scattering (figure 1C) and absorption (figure 1D) can be obtained and characterized. Supplementary table S2 shows all spatially averaged values of DOSI outcome variables.

Figure 2 shows sequential images of four parameters in one representative male subject, with corresponding weights shown above. Qualitative analysis of images from this subject demonstrates a gradient in A, with higher baseline values measured in proximity to the abdominal midline, corresponding to areas of thicker subcutaneous AT. Measurement locations in the upper row tend to exhibit higher values of A, and larger increases in A. Both water fraction and [HbR] appear to increase diffusely, particularly in lateral locations.

NIR Scattering Changes

At each measurement point, two parameters related to optical scattering were obtained by measuring reduced scattering coefficients at all four wavelengths, according to equation 2 (32):

$$\mu_s' = A\left(\frac{\lambda}{500nm}\right)^b$$

Here, *b* is the unitless "slope" parameter which describes the dependence of scattering on wavelength, while *A* is a factor in mm^{-1} units corresponding to amplitude of NIR scattering. The λ term is the wavelength at which μ_s' is measured, and the 500 nm term is a reference wavelength used for normalization (32). In figure 3A, serial average scattering spectra in one participant are shown. Here, there is both an upward shift in the spectrum with weight loss, as well as steepening of the curve with respect to wavelength. These observations would therefore constitute an increase in *A* and a decrease in *b*.

From T0 to T12, *A* increased by 17.0 ± 8.4 % (mean ± SD) and ranged from +2.9% to +28.7%.The mean *b* parameter change was −24.4 ± 20.9 %, ranging from + 1.0% to −68.5%. *A* was significantly higher at both T6 (Figure 4A, T6-T0 = 0.15 ± 0.04 mm^{-1}, adj. $p = 0.002$) and T12 (T12 – T6 = 0.08 ± 0.03 mm^{-1}, adj. $p = 0.007$, T12-T0 = 0.23 ± 0.04 mm^{-1}, adj. $p < 0.001$). The *b* parameter was significantly more negative at T6 and T12 than T0 (Figure 4B, T6 – T0 = −0.12 ± 0.03, adj. $p = 0.001$, T12 – T6 = −0.06 ± 0.02, adj. $p = 0.040$, T12 – T0 = −0.17 ± 0.04, adj. $p < 0.001$). Both parameters changed more between T0 and T6 than between T6 and T12.

Absorption changes

Inspection of absorption spectra measured in individuals revealed progressive upward shifts in the 950–1000 nm range where water is the primary absorber (as shown in one representative subject, Fig. 3B). Model coefficients for CR on absorption parameters are shown in Table S1. [HbO_2] was significantly higher at T12 than T0 (Fig. 4C, T12 – T0 = 2.0 ± 0.8 μM, adj. $p = 0.019$). The mean [HbR] was higher at T12 and T6 than T0 (figure 4D, T6 – T0 = 0.6 ± 0.1 μM, adj. $p < 0.001$, T12 – T0 = 1.1 ± 0.3 μM, adj. $p < 0.001$, T12 – T6 = 0.5 ± 0.2 μM, adj. $p = 0.051$). [THb] was higher at T12 than at both T6 and T0 (figure 4E, T12 – T0 = 3.2 ± 0.8 μM, adj. $p < 0.001$, T12 – T6 = 2.1 ± 0.8 μM, adj. $p = 0.026$). The mean tissue water fraction increased from T0 to T6 (figure 4F, T6 – T0 = 3.4 ± 1.0%, adj. $p = 0.003$), and from T6 to T12 (T12 – T6 = 3.9 ± 0.6%, adj. $p < 0.001$, T12 – T0 = 7.2 ± 1.1%, adj. $p < 0.001$). No significant associations were found between CR and stO_2 or lipid content. Individual responses for each optical outcome are shown in supplementary table 2.

Correlations between optical measures and weight loss

A significant Pearson correlation was found between the magnitude of weight loss and the increase in tissue water content in individual subjects between T0 and T12 (Figure 5, r = 0.679, $p = 0.031$).

Discussion

AT structure and optical scattering

It is known that adipocyte size is dynamic, and that it is positively associated with degree of obesity, as well as fasting insulin levels (37). A recent study of twins non-concordant for obesity showed that increased weight correlates with larger adipocytes, with or without AT hyperplasia (38). The response of adipocytes to weight loss interventions has also been observed experimentally. A study in humans has shown that individuals subjected to 12 weeks of a very low calorie diet (< 3400 kJ/day) show adipocyte volume reductions on the order of 15–20% (13). Over this time scale, it is unlikely that a change in subcutaneous AT cell number would be observed (13), although AT hyperplasia is seen in obesity (39). It has also been observed that weight loss of 5% of total body weight is sufficient to reduce adipocyte size in severely obese women (40).

Based on the magnitude of weight loss observed in our study (11.7 ± 3.4 % of starting weight, T0 to T12) and the time course, we can postulate that the increases in NIR scattering amplitude (mean + 17.0% from T0 to T12) observed are related to a reduction in adipocyte size. In the NIR range (650–1000 nm), the light scattering parameters "A" and "b" correspond to the distributions of density and size of scattering particles (41, 42), respectively, that are comparable in dimension to the optical wavelength (32, 43). Therefore, reduction in adipocyte volume associated with CR likely leads to several effects: 1) an increase in the density of subcellular contributors to scattering per unit volume due to relatively reduced cytoplasm; 2) increased density of extracellular matrix (ECM, e.g. collagen); and 3) a larger preponderance of subcellular structures (possibly mitochondria, or more vesicles for mobilization of lipids into the bloodstream) and ECM contributing to the scattering signal. The first two processes would be expected to increase the density of scattering particles, and therefore produce an increase in A. The third process would be likely to produce a shift toward a smaller average size of scattering particle, and therefore an increase in the magnitude of b (i.e. a more negative scattering slope).

Although the precise biological interpretation of these measurements would require histopathological examination of biopsied tissue, our interpretation can be placed in the context of previously published non-invasive studies examining breast scattering properties, which is composed of varying proportions of adipose, glandular, and ECM tissue. Generally, these studies have shown that the scattering parameters of breast adipose tissue are similar to the baseline AT measurements we report here (44). In addition, the magnitudes of A and b increase in more dense, pre-menopausal breast, which includes increasing proportions of organelle- and collagen-rich tissues (44, 45), much like A and b magnitudes increase in AT measurements of CR subjects. Additionally, it has been observed that post-menopausal breast tissue in subjects receiving estrogen replacement therapy demonstrates higher scattering values, possibly related to increased metabolic activity (46). While breast physiology is much different than that of subcutaneous fat, these previous observations lend support to the interpretation that the scattering changes we observed with CR are related to increased AT density and perhaps metabolic activation.

The specific cellular or extracellular components corresponding to these scattering particles are not precisely known. However, it has been shown both theoretically and experimentally that membrane-bound organelles, such as vesicles or mitochondria contribute to scattering signals due to the changes in refractive indices across their membranes (43, 47–49). Other possibilities for organelles contributing to increased scattering include a higher rate of adipocyte pinocytosis and therefore a larger proportion of membrane-bound vesicles (50). However, this is merely speculative, and to determine the precise source of the scattering changes, further controlled studies incorporating histology and microscopy are needed. Nevertheless, to our knowledge, these findings represent the first *in vivo* characterization of NIR scattering properties of AT in the context of weight loss.

Changes in AT NIR absorption parameters

Analysis of absorption spectra revealed that CR is associated with significant increases in tissue [HbO_2], [HbR], [THb], and water fraction, which reflect perfusion, O_2 delivery, and hydration. It is known that obesity suppresses AT blood flow at rest (7), and blunts the post-prandial increase in flow (51), but the implications of this reduction are not fully known. Interestingly, subcutaneous AT P_{O2} has been found to be elevated in obesity by direct measurement, possibly reflecting an O_2 extraction deficit (5). While subcutaneous AT O_2 consumption is low compared to other tissues, there is evidence for the relevance of AT hypoxia in the progression of obesity (7). Furthermore, as described previously, increased oxidative capacity is a feature of brown and beige adipocytes, both of which are associated with improvements in metabolic status. Much about the relationship between diet status, inflammation, and AT metabolism in humans is unknown, largely due to difficulties involved in measuring AT blood flow and P_{O2}.

While DOSI does not directly measure these quantities, the changes observed in this study suggest that subcutaneous AT responds to weight loss with an increase in O_2 extraction ([HbR]), and water content at the bulk tissue level. Weight loss by CR has been shown to decrease total body water content, with an increase in the ratio of extracellular to intracellular water (52), partly due to the early mobilization of glycogen stores (52). There is comparatively little known about AT hydration status. A 2003 study used skin surface measurements of dielectric constant to show that that subcutaneous AT water content increases with weight loss by CR (53). The authors attributed this increase to higher blood flow and nutrient delivery, and also correlated it with an improvement in insulin sensitivity (53). The fact that we observed an increase in AT [THb] along with water content would seem to support this previous conclusion. Finally, there was a significant correlation within subjects between the percentage of weight lost and the mean increase in water fraction from T0 to T12 (Figure 5). It is not clear why the magnitude of change in water content appears to uniquely correlate with the degree of weight loss. However, the fact that this analysis was performed by averaging changes at all measurement locations likely obscures some correlations which might be detected by other signals. It is also possible that tissue water content is the parameter most closely related to the reduction in AT fat mass that occurs with weight loss, but this must be confirmed with more data. While we cannot comment on the relative contributions of extracellular vs. intracellular water to the overall increase, DOSI may be sensitive to compartment-specific hydration (54). For example, in optical

mammography, the tissue water fraction has been suggested to be reflective mostly of extravascular fluid (44), which we expect to increase in a manner that compensates for the degree of loss of lipid volume in AT during CR.

Because [HbR] changes are known to be a consequence of O_2 extraction (22, 55), the observed [HbR] increase likely reflects enhanced AT O_2 extraction. This is consistent with our observation of changes in *A* and *b* scattering parameters that suggest a reduction in adipocyte size with weight loss. Adipocyte shrinkage is thought to reduce the O_2 diffusion distance to mitochondria (7), potentiating extraction. However, there are many other factors that influence AT O_2 flux. For example, recent data showed that an early effect of a high fat diet in mice is increased AT O_2 consumption driven by mitochondrial uncoupling (6). This leads to relative hypoxia and HIF-1α mediated inflammation, a phenomenon implicated in insulin resistance (6). Our measurements of increased [HbR] with CR seem to be in contradiction with these findings, but only if the increased [HbR] is reflective of an increase in individual adipocyte O_2 extraction. To resolve this issue would require a measurement of intrinsic AT cellular O_2 consumption, as has been done recently using related optical techniques in human skin (56).

Ultrasound measurements and photon penetration

To verify that detected signals were derived primarily from subcutaneous AT and not underlying abdominal musculature, Monte Carlo simulations of tissue light propagation were performed. These revealed that with the measurement scheme used in this study and a subcutaneous thickness of 10 mm, the distribution of photon paths would result in a mean interrogation depth of 5–6 mm with less than 4% of the total detected photons reaching the muscle layer. Given that the measured values of subcutaneous AT thickness were always greater than 10 mm, we expect negligible contribution to DOSI signals from deeper tissue components. Furthermore, though AT thickness decreased during weight loss, the significant increase in scattering cannot be physiologically explained by additional contributions from muscle because muscle exhibits lower scattering than AT.

These results suggest that DOSI is sensitive to AT structural and metabolic changes during CR. However, this study has several limitations. First, histology could not be performed, and we must therefore rely on known effects of CR on AT observed by others. Second, the small sample size thus far (n = 10) does not permit analysis of correlations between changes in DOSI parameters and baseline individual characteristics. An additional concern is the long interval between measurements (six weeks). Animal studies show that AT O_2 consumption changes within days after a diet intervention (6), and adipocyte size increases have been observed in several days as well (14). Finally, future studies must also explore the contribution of abdominal spatial heterogeneity on the changes described using customized statistical methods.

These limitations notwithstanding, our data demonstrate that DOSI-detected changes in AT optical properties are consistent with existing hypotheses on the response of AT to CR and weight loss. DOSI or similar techniques may contribute to a fuller understanding of AT physiology in various metabolic states, and may constitute a new bedside tool for monitoring AT metabolism and composition.

Supplementary Material

Refer to Web version on PubMed Central for supplementary material.

Acknowledgments

Funding: This research was supported by an NIH TL-1 training fellowship to GG (NIH 8UL1TR000153), an NIH CTSA grant (NIH UL1 TR000153) and NIH P41EB015890, the Laser Microbeam and Medical Program, LAMMP). Additional support was also provided by the Arnold and Mabel Beckman Foundation. We gratefully acknowledge the administration of the UC Irvine weight management program for facilitating recruitment of research subjects. We also acknowledge Amanda Durkin and Keunsik No for construction of DOSI instrumentation, and Brian Hill for development of DOSI data processing methods.

References

1. Bremer AA, Jialal I. Adipose tissue dysfunction in nascent metabolic syndrome. J Obes. 2013; 2013(393192):1–8.
2. Bremer AA, Devaraj S, Afify A, Jialal I. Adipose tissue dysregulation in patients with metabolic syndrome. J Clin Endocrinol Metab. 2011; 96(11):E1782–E1788. [PubMed: 21865369]
3. Bassaganya-Riera J, Misyak S, Guri AJ, Hontecillas R. PPAR gamma is highly expressed in F4/80(hi) adipose tissue macrophages and dampens adipose-tissue inflammation. Cell Immunol. 2009; 258(2):138–146. [PubMed: 19423085]
4. Le KA, Mahurkar S, Alderete TL, Hasson RE, Adam TC, Kim JS, et al. Subcutaneous adipose tissue macrophage infiltration is associated with hepatic and visceral fat deposition, hyperinsulinemia, and stimulation of NF-{kappa}B stress pathway. Diabetes. 2011; 60(11):2802–2809. [PubMed: 22025778]
5. Goossens GH, Bizzarri A, Venteclef N, Essers Y, Cleutjens JP, Konings E, et al. Increased adipose tissue oxygen tension in obese compared with lean men is accompanied by insulin resistance, impaired adipose tissue capillarization, and inflammation. Circulation. 2011; 124(1):67–76. [PubMed: 21670228]
6. Lee YS, Kim JW, Osborne O, Oh da Y, Sasik R, Schenk S, et al. Increased adipocyte O2 consumption triggers HIF-1alpha, causing inflammation and insulin resistance in obesity. Cell. 2014; 157(6):1339–1352. [PubMed: 24906151]
7. Hodson L, Humphreys SM, Karpe F, Frayn KN. Metabolic signatures of human adipose tissue hypoxia in obesity. Diabetes. 2013; 62(5):1417–1425. [PubMed: 23274888]
8. Pasarica M, Sereda OR, Redman LM, Albarado DC, Hymel DT, Roan LE, et al. Reduced adipose tissue oxygenation in human obesity: evidence for rarefaction, macrophage chemotaxis, and inflammation without an angiogenic response. Diabetes. 2009; 58(3):718–725. [PubMed: 19074987]
9. Samuvel DJ, Jin J, Sundararaj KP, Li Y, Zhang X, Lopes-Virella MF, et al. TLR4 activation and IL-6-mediated cross talk between adipocytes and mononuclear cells synergistically stimulate MMP-1 expression. Endocrinology. 2011; 152(12):4662–4671. [PubMed: 21952248]
10. Karolina DS, Armugam A, Tavintharan S, Wong MT, Lim SC, Sum CF, et al. MicroRNA 144 impairs insulin signaling by inhibiting the expression of insulin receptor substrate 1 in type 2 diabetes mellitus. PLoS One. 2011; 6(8):e22839. [PubMed: 21829658]
11. Bordone L, Guarente L. Calorie restriction, SIRT1 and metabolism: understanding longevity. Nat Rev Mol Cell Biol. 2005; 6(4):298–305. [PubMed: 15768047]
12. Nisoli E, Tonello C, Cardile A, Cozzi V, Bracale R, Tedesco L, et al. Calorie restriction promotes mitochondrial biogenesis by inducing the expression of eNOS. Science. 2005; 310(5746):314–317. [PubMed: 16224023]
13. Rossmeislova L, Malisova L, Kracmerova J, Stich V. Adaptation of human adipose tissue to hypocaloric diet. Int J Obes (Lond). 2013; 37(5):640–650. [PubMed: 22641066]
14. Verhoef SP, Camps SG, Bouwman FG, Mariman EC, Westerterp KR. Physiological response of adipocytes to weight loss and maintenance. PLoS One. 2013; 8(3):e58011. [PubMed: 23505452]

15. Jo J, Shreif Z, Periwal V. Quantitative dynamics of adipose cells. Adipocyte. 2012; 1(2):80–88. [PubMed: 23700516]
16. Cotillard A, Poitou C, Torcivia A, Bouillot JL, Dietrich A, Kloting N, et al. Adipocyte size threshold matters: link with risk of type 2 diabetes and improved insulin resistance after gastric bypass. J Clin Endocrinol Metab. 2014; 99(8):E1466–E1470. [PubMed: 24780048]
17. Landgraf K, Rockstroh D, Wagner IV, Weise S, Tauscher R, Schwartze JT, et al. Evidence of early alterations in adipose tissue biology and function and its association with obesity-related inflammation and insulin resistance in children. Diabetes. 2015; 64(4):1249–1261. [PubMed: 25392242]
18. Lemoine AY, Ledoux S, Larger E. Adipose tissue angiogenesis in obesity. Thromb Haemost. 2013; 110(4):661–668. [PubMed: 23595655]
19. Trayhurn P. Hypoxia and adipose tissue function and dysfunction in obesity. Physiol Rev. 2013; 93(1):1–21. [PubMed: 23303904]
20. Wu J, Bostrom P, Sparks LM, Ye L, Choi JH, Giang AH, et al. Beige adipocytes are a distinct type of thermogenic fat cell in mouse and human. Cell. 2012; 150(2):366–376. [PubMed: 22796012]
21. Bartelt A, Heeren J. Adipose tissue browning and metabolic health. Nat Rev Endocrinol. 2014; 10(1):24–36. [PubMed: 24146030]
22. Tromberg, BJ.; Cerussi, AE.; Chung, SH.; Tanamai, W.; Durkin, A. Broadband diffuse pptical spectroscopy and imaging. In: Boas, DA.; Pitris, C.; Ramanujam, N., editors. Handbook of Biomedical Optics. London, UK: CRC press; 2012. p. 181-193.
23. No KS, Kwong R, Chou PH, Cerussi A. Design and testing of a miniature broadband frequency domain photon migration instrument. J Biomed Opt. 2008; 13(5):050509. [PubMed: 19021379]
24. Bevilacqua F, Berger AJ, Cerussi AE, Jakubowski D, Tromberg BJ. Broadband absorption spectroscopy in turbid media by combined frequency-domain and steady-state methods. Appl Opt. 2000; 39(34):6498–6507. [PubMed: 18354663]
25. Lee J, Kim JG, Mahon S, Tromberg BJ, Ryan KL, Convertino VA, et al. Tissue hemoglobin monitoring of progressive central hypovolemia in humans using broadband diffuse optical spectroscopy. J Biomed Opt. 2008; 13(6):064027. [PubMed: 19123673]
26. Pierro ML, Sassaroli A, Bergethon PR, Ehrenberg BL, Fantini S. Phase-amplitude investigation of spontaneous low-frequency oscillations of cerebral hemodynamics with near-infrared spectroscopy: a sleep study in human subjects. NeuroImage. 2012; 63(3):1571–1584. [PubMed: 22820416]
27. Chin LM, Kowalchuk JM, Barstow TJ, Kondo N, Amano T, Shiojiri T, et al. The relationship between muscle deoxygenation and activation in different muscles of the quadriceps during cycle ramp exercise. J Appl Physiol (1985). 2011; 111(5):1259–1265. [PubMed: 21799133]
28. Cerussi A, Shah N, Hsiang D, Durkin A, Butler J, Tromberg BJ. In vivo absorption, scattering, and physiologic properties of 58 malignant breast tumors determined by broadband diffuse optical spectroscopy. J Biomed Opt. 2006; 11(4):044005. [PubMed: 16965162]
29. O'Sullivan TD, Leproux A, Chen JH, Bahri S, Matlock A, Roblyer D, et al. Optical imaging correlates with magnetic resonance imaging breast density and reveals composition changes during neoadjuvant chemotherapy. Breast Cancer Res. 2013; 15(5):R89. [PubMed: 24066941]
30. Roblyer D, Ueda S, Cerussi A, Tanamai W, Durkin A, Mehta R, et al. Optical imaging of breast cancer oxyhemoglobin flare correlates with neoadjuvant chemotherapy response one day after starting treatment. Proc Natl Acad Sci U S A. 2011; 108(35):14626–14631. [PubMed: 21852577]
31. Martinelli M, Gardner A, Cuccia D, Hayakawa C, Spanier J, Venugopalan V. Analysis of single Monte Carlo methods for prediction of reflectance from turbid media. Opt express. 2011; 19(20): 19627–19642. [PubMed: 21996904]
32. Jacques SL. Optical properties of biological tissues: a review. Phys Med Biol. 2013; 58(11):R37–R61. [PubMed: 23666068]
33. Matsushita K, Homma S, Okada E. Influence of adipose tissue on muscle oxygenation measurement with an NIRS instrument. Proc SPIE Int Soc Opt Eng. 1998; 3194:159–165.
34. Bates D, Mächler M, Bolker B, Walker S. Fitting linear mixed-effects models using lme4. arXiv preprint. 2014 *arXiv:1406.5823*.

35. Li, Y.; Baron, J. Linear mixed-effects models in analyzing repeated-measures data. In: Li, Y.; Baron, J., editors. Behavioral Research Data Analysis with R. New York, New York, USA: Springer New York; 2012. p. 177-204.
36. Baayen RH, Davidson DJ, Bates DM. Mixed-effects modeling with crossed random effects for subjects and items. Journal of Memory and Language. 2008; 59(4):390–412.
37. Bjorntorp P, Gustafson A, Persson B. Adipose tissue fat cell size and number in relation to metabolism in endogenous hypertriglyceridemia. Acta Med Scand. 1971; 190(5):363–367. [PubMed: 5149263]
38. Heinonen S, Saarinen L, Naukkarinen J, et al. Adipocyte morphology and implications for metabolic derangements in acquired obesity. Int J Obes (Lond). 2014; 38(11):1423–1431. [PubMed: 24549139]
39. Arner P, Spalding KL. Fat cell turnover in humans. Biochem Biophys Res Commun. 2010; 396(1): 101–104. [PubMed: 20494119]
40. Varady KA, Tussing L, Bhutani S, Braunschweig CL. Degree of weight loss required to improve adipokine concentrations and decrease fat cell size in severely obese women. Metabolism. 2009; 58(8):1096–1101. [PubMed: 19477470]
41. Schmitt JM, Kumar G. Optical scattering properties of soft tissue: a discrete particle model. Appl Opt. 1998; 37(13):2788–2797. [PubMed: 18273225]
42. Coquoz O, Svaasand LO, Tromberg BJ. Optical property measurements of turbid media in a small-volume cuvette with frequency-domain photon migration. Appl Opt. 2001; 40(34):6281–6291. [PubMed: 18364934]
43. Bartek M, Wang X, Wells W, Paulsen KD, Pogue BW. Estimation of subcellular particle size histograms with electron microscopy for prediction of optical scattering in breast tissue. J Biomed Opt. 2006; 11(6):064007. [PubMed: 17212530]
44. Srinivasan S, Pogue BW, Jiang SD, Dehghani H, Kogel C, Soho S, et al. Interpreting hemoglobin and water concentration, oxygen saturation, and scattering measured in vivo by near-infrared breast tomography. Proc Natl Acad Sci U S A. 2003; 100(21):12349–12354. [PubMed: 14514888]
45. Cerussi AE, Berger AJ, Bevilacqua F, Shah N, Jakubowski D, Butler J, et al. Sources of absorption and scattering contrast for near-infrared optical mammography. Acad Radiol. 2001; 8(3):211–218. [PubMed: 11249084]
46. Shah N, Cerussi A, Eker C, Espinoza J, Butler J, Fishkin J, et al. Noninvasive functional optical spectroscopy of human breast tissue. Proc Natl Acad Sci U S A. 2001; 98(8):4420–4425. [PubMed: 11287650]
47. Wang X, Pogue BW, Jiang S, Dehghani H, Song X, Srinivasan S, et al. Image reconstruction of effective Mie scattering parameters of breast tissue in vivo with near-infrared tomography. J Biomed Opt. 2006; 11(4):041106. [PubMed: 16965134]
48. Beauvoit B, Evans SM, Jenkins TW, Miller EE, Chance B. Correlation between the light scattering and the mitochondrial content of normal tissues and transplantable rodent tumors. Anal Biochem. 1995; 226(1):167–174. [PubMed: 7785769]
49. Beauvoit B, Kitai T, Chance B. Contribution of the mitochondrial compartment to the optical properties of the rat liver: a theoretical and practical approach. Biophysical J. 1994; 67(6):2501–2510.
50. Barrnett RJ, Ball EG. Metabolic and ultrastructural changes induced in adipose tissue by insulin. J Biophys Biochem Cytol. 1960; 8:83–101. [PubMed: 13687312]
51. Frayn KN, Karpe F. Regulation of human subcutaneous adipose tissue blood flow. Int J Obes (Lond). 2014; 38(8):1019–1026. [PubMed: 24166067]
52. Siervo M, Faber P, Gibney ER, et al. Use of the cellular model of body composition to describe changes in body water compartments after total fasting, very low calorie diet and low calorie diet in obese men. Int J Obes (Lond). 2010; 34(5):908–918. [PubMed: 20142822]
53. Laaksonen DE, Nuutinen J, Lahtinen T, Rissanen A, Niskanen LK. Changes in abdominal subcutaneous fat water content with rapid weight loss and long-term weight maintenance in abdominally obese men and women. Int J Obes Relat Metab Disord. 2003; 27(6):677–683. [PubMed: 12833111]

54. Chung SH, Yu H, Su MY, Cerussi AE, Tromberg BJ. Molecular imaging of water binding state and diffusion in breast cancer using diffuse optical spectroscopy and diffusion weighted MRI. J Biomed Opt. 2012; 17(7):071304. [PubMed: 22894465]

55. Ferrari M, Muthalib M, Quaresima V. The use of near-infrared spectroscopy in understanding skeletal muscle physiology: recent developments. Philos Transact A Math Phys Eng Sci. 2011; 369(1955):4577–4590.

56. Balu M, Mazhar A, Hayakawa CK, Mittal R, Krasieva TB, Konig K, et al. In vivo multiphoton NADH fluorescence reveals depth-dependent keratinocyte metabolism in human skin. Biophysical journal. 2013; 104(1):258–267. [PubMed: 23332078]

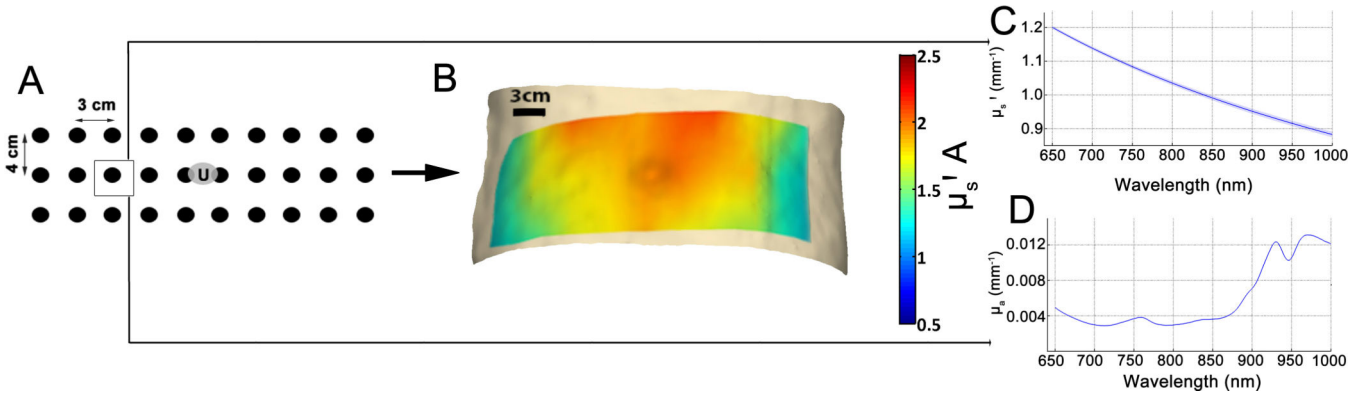

Figure 1. Schematic of DOSI measurement procedure

(A) demonstrates the grid used with distances between points indicated. The “U” in the center of the grid refers to the subject’s umbilicus. (B) shows a typical scattering spectrum obtained from one subject at point M3, with the mean of three replicate measurements ± SD shown as a line and a shaded area respectively. (C) shows the mean absorption spectrum at the same location in the same subject, also as mean ± SD (D) demonstrates example heat maps of scattering and absorption parameters from one subject over all 30 measurement points with linear interpolation.

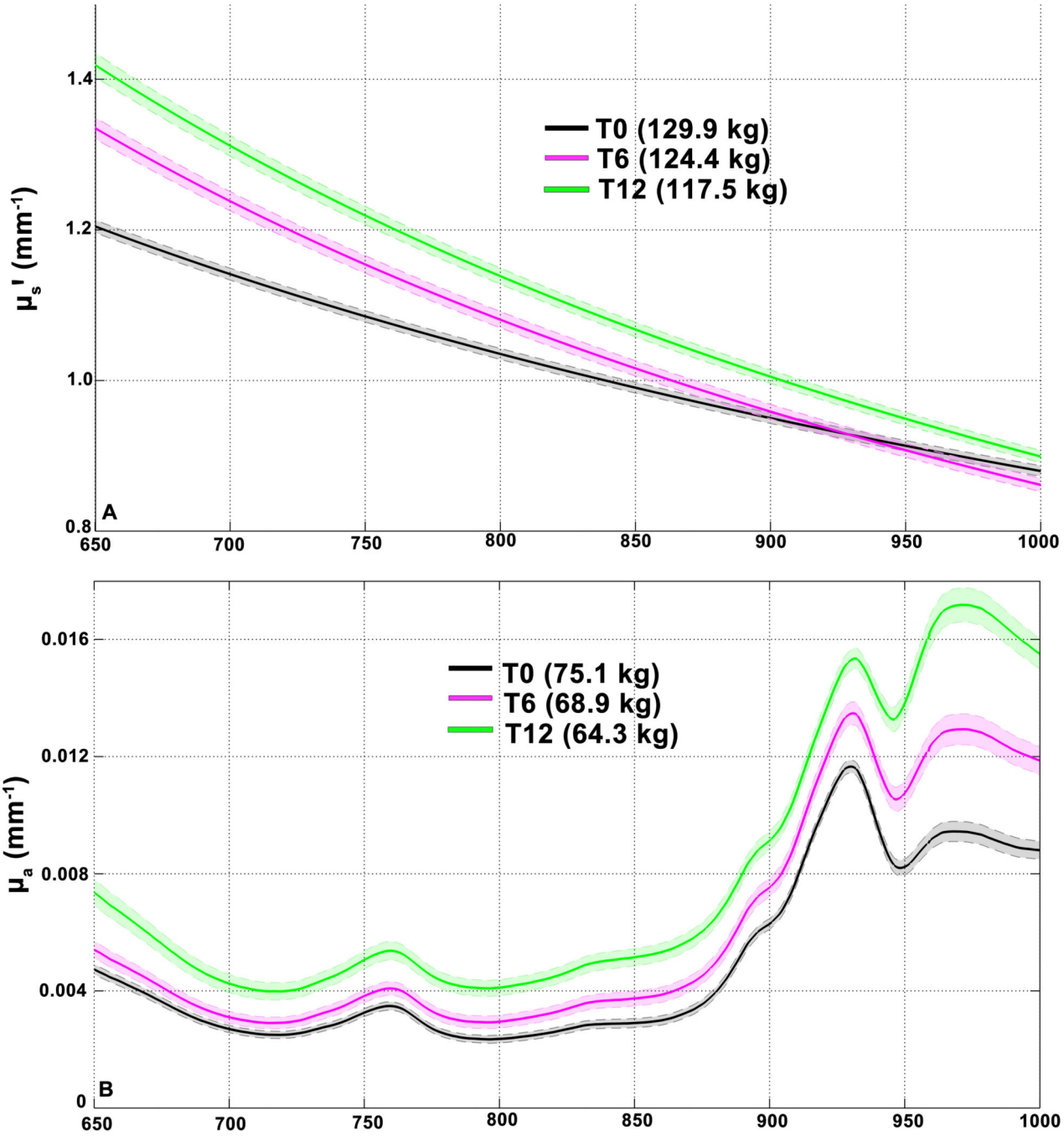

Figure 2. Individual subject DOSI maps

Serial images of DOSI parameters in one male subject overlayed on 3-D images of a representative abdomen. Corresponding measured weight at each respective time point is also shown. (A) shows serial images of μ_s' *A* parameter, (B) shows μ_s' *b*, (C) shows tissue water fraction, and (D) shows [HbR]. Heat maps have been overlayed onto a representative 3D abdominal image for visualization only, and these do not represent subject abdominal shape or contour.

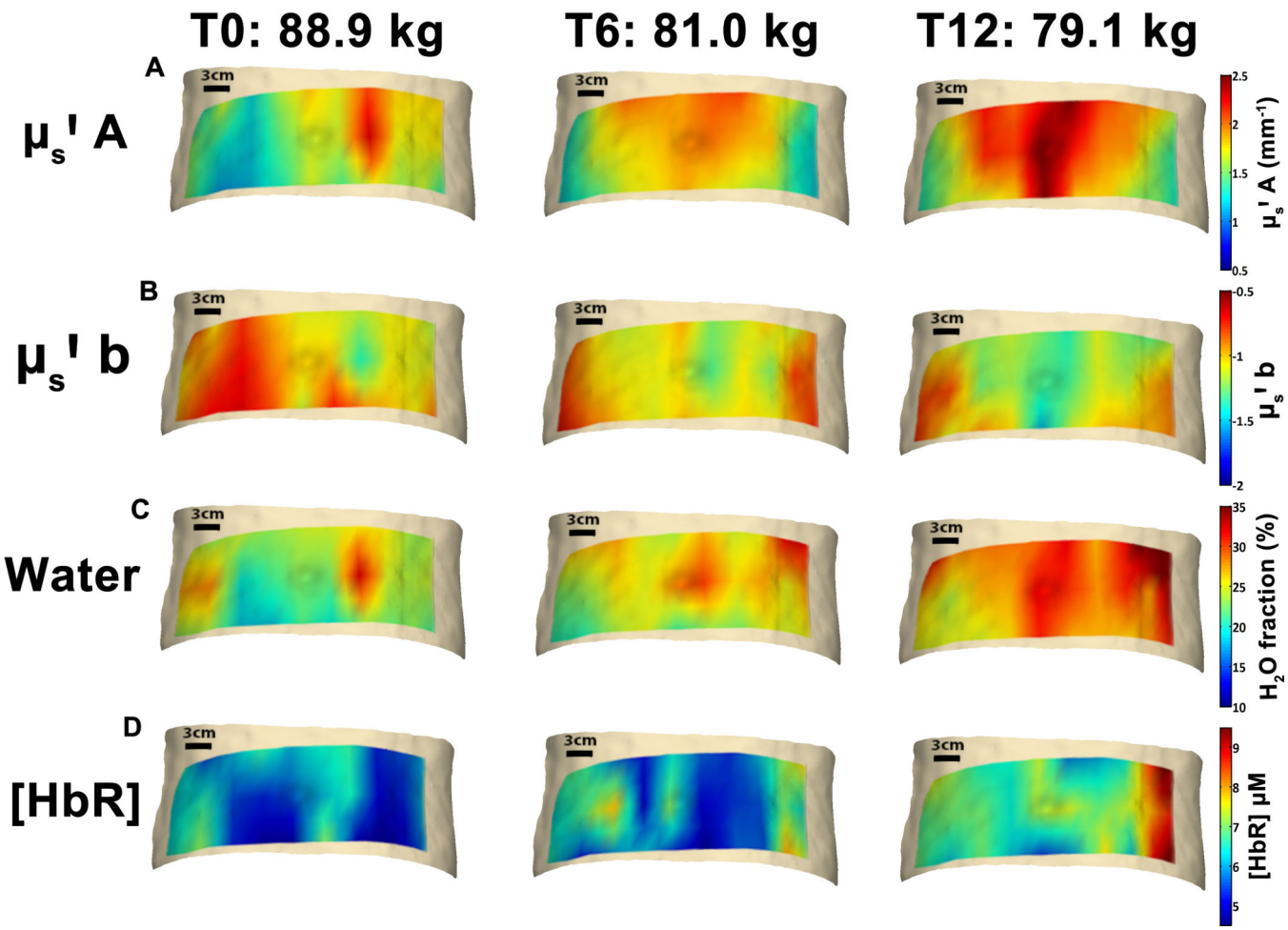

Figure 3. Individual Average Optical Spectra

Mean ± SEM of optical properties in two different subjects over the whole experimental period. In both plots, the x-axis corresponds to wavelength in nm, over the range of the DOSI measurement (650–1000 nm) (A) shows mean ± SD μ_s' over 29 (one excluded from this subject) measurement points at T0 (black), T6 (magenta) and T12 (green). Corresponding subject weights at these points are shown in legend. (B) shows mean ± SD of 30 measurement points of μ_a in another subject. Both coefficients are expressed in units of inverse millimeters.

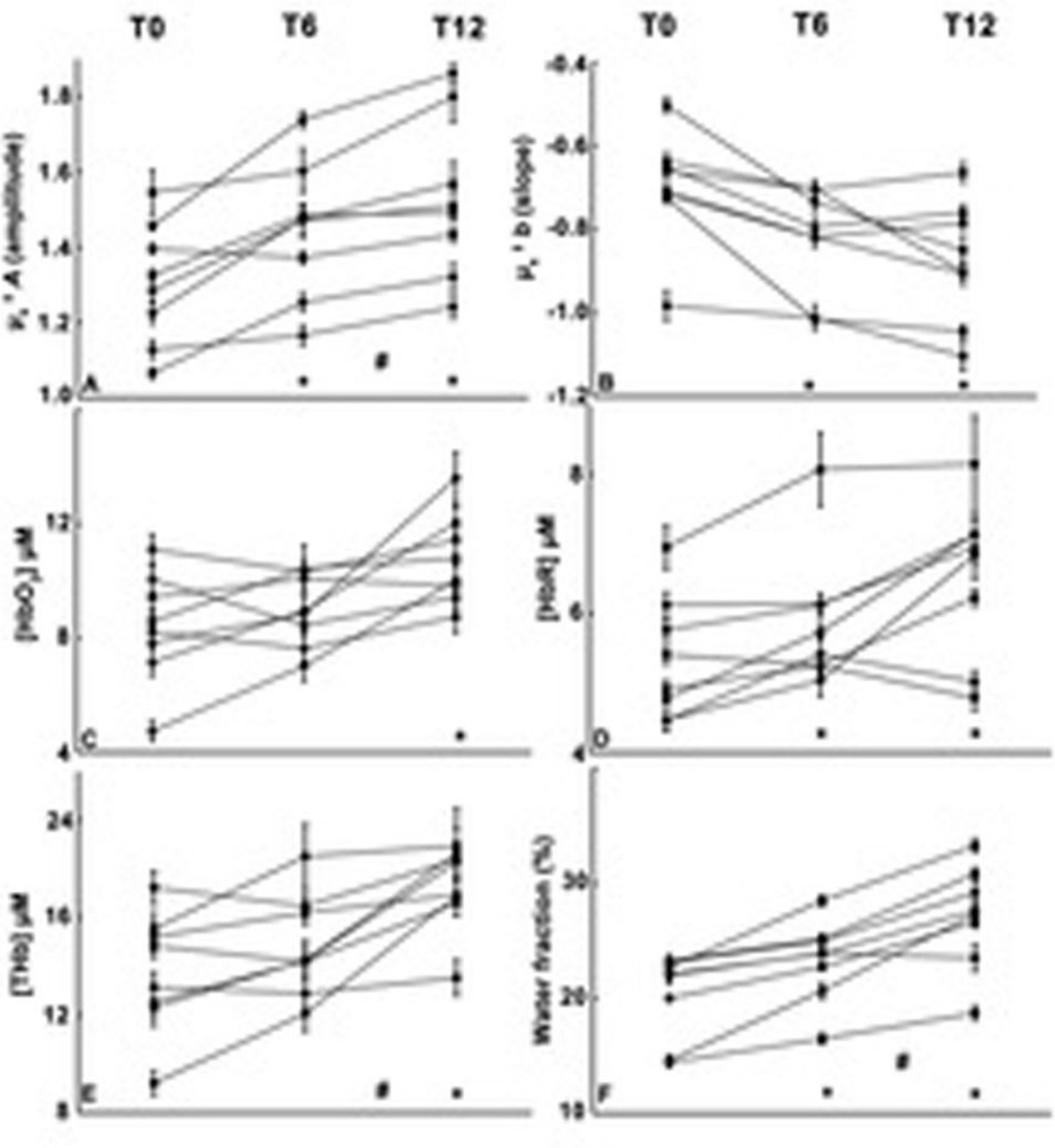

Figure 4. Mean optical parameter values

Individual subject profiles of scattering and absorption derived parameters for all 10 subjects at three time points. (A) and (B) panels are *A* and *b* scattering parameters, respectively. (C) is [HbO2], (D) is [HbR], (E) [THb], (F) water fraction, with units indicated on respective Y axes. Each individual point represents the mean of all measurement locations obtained, and error bars are standard errors for all measurement points obtained. * symbol indicates a significant difference in mean value for all participants from T0 level, whereas # indicates a significant difference between T6 and T12.

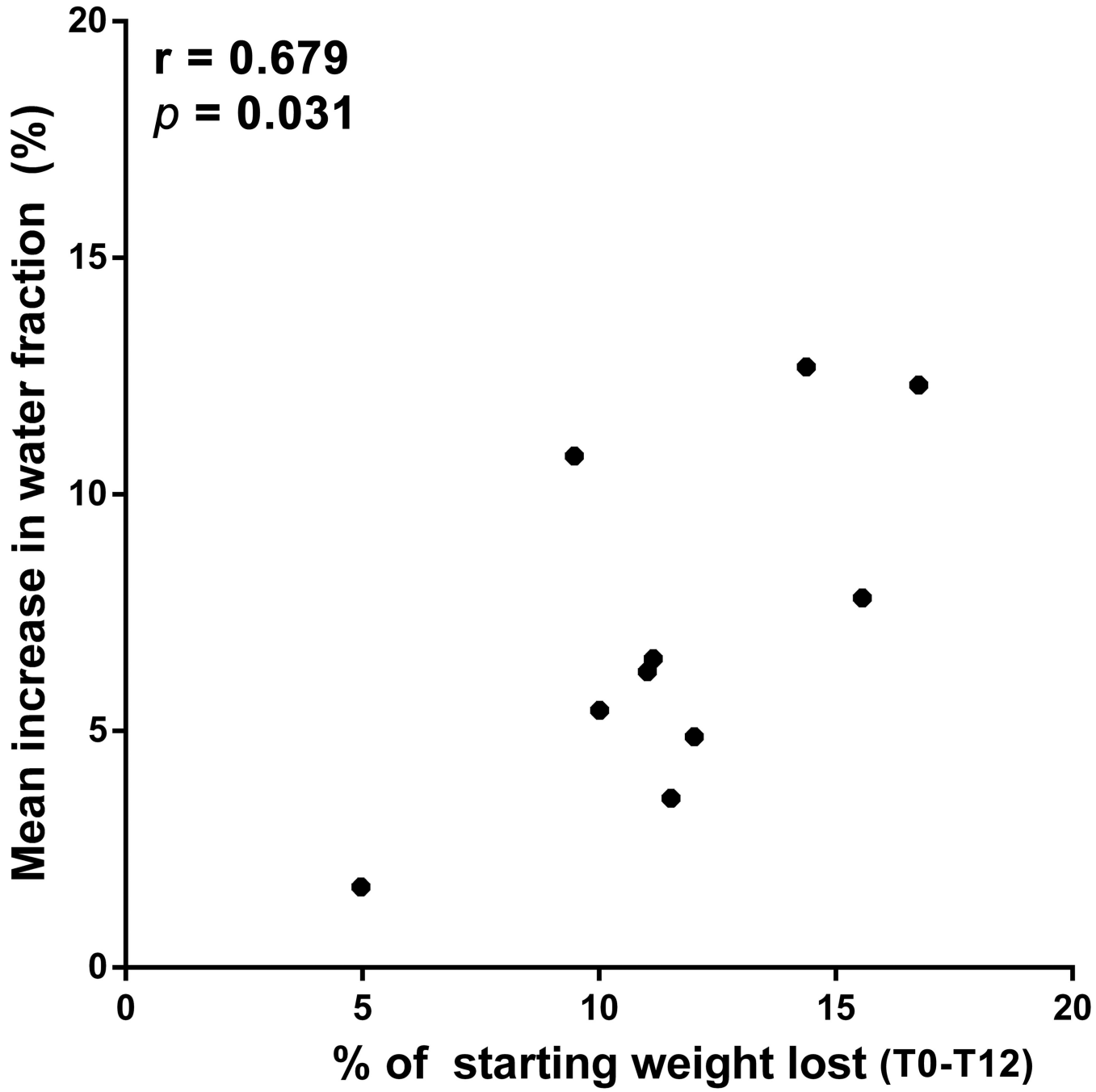

Figure 5. Correlation between water content and weight loss

Pearson Product-Moment Correlation beween individual subject weight loss magnitude and absolute change in water (A) from T0 to T12. Pearson coefficient and corresponding p-value are shown.

Int J Obes (Lond). Author manuscript; available in PMC 2016 October 22.

Table 1

Subject anthropometric data and blood pressure

Participant anthropometric data at each measurement session. P-values are shown for Wilcoxon signed-rank test for effect of CR.

					Weight (kg)			Abd. Circumference (cm)			Systolic BP (mm Hg)			Diastolic BP (mm Hg)		
Subject	**Gender**	**Age**	**Diet**	**T1 BMI**	**T1**	**T2**	**T3**	**T1**	**T2**	**T3**	**T1**	**T2**	**T3**	**T1**	**T2**	**T3**
1	M	73	1	42.7	151.0	139.9	127.5	137	130	125	127	113	107	78	71	73
2	M	49	1	36.7	129.8	124.4	117.5	121	113	113	126	122	126	78	79	82
3	M	58	1	33.7	109.5	98.9	97.3	106	106	100	122	115	107	83	73	70
4	F	58	2	30.3	75.1	68.9	64.3	99	90	80	131	126	124	89	78	80
5	F	45	1	40.0	115.9	108.4	104.3	127	119	117	127	122	130	89	85	80
6	F	60	1	29.9	86.6	79.2	76.2	100	98	95	114	107	116	69	71	76
7	F	58	2	25.2	64.4	63.0	61.2	88	86	83	120	102	111	75	66	72
8	M	41	2	31.6	88.9	81.0	79.1	99	93	93	139	135	127	92	94	87
9	M	58	1	31.2	110.4	95.5	91.9	107	99	93	138	115	121	91	83	76
10	F	60	1	32.4	86.8	80.7	76.8	108	103	98	139	138	128	92	76	72
mean		**56**		**33.4**	**101.8**	**94.0**	**89.6**	**109**	**104**	**100**	**128**	**120**	**120**	**84**	**78**	**77**
SD		9		5	26	25	22	15	14	14	9	11	9	8	8	5
SEM		2.8		2	8	8	7	5	4	5	3	4	3	3	3	2
					T2-T1	T3-T1	T3-T2	T2-T1	T3-T1	T3-T2	T2-T1	T3-T1	T3-T2	T2-T1	T3-T1	T3-T2
p					**0.006**	**0.006**	**0.006**	**0.027**	**0.017**	**0.042**	**0.017**	0.073	1.000	0.097	0.124	1.000
mean (M)	M	56		35.2	117.9	107.9	102.7	114	108	105	130	120	118	84	80	78
mean (F)	F	56		31.5	85.8	80.0	76.6	104	99	95	126	119	122	83	75	76